ICES Journal of Marine Science

ICES Journal of Marine Science (2020), 77(4), 1556–1572. doi:10.1093/icesjms/fsaa067

Contribution to the Themed Section: '*Science in support of a nonlinear non-equilibrium world*'

Original Article

Stability and resilience in a nutrient-phytoplankton marine ecosystem model

Žarko Kovač[1]*, Trevor Platt[2], and Shubha Sathyendranath[3]

[1]*Department of Physics, Faculty of Science, University of Split, Ruđera Boškovića 33, 21000 Split, Croatia*
[2]*Plymouth Marine Laboratory, Prospect Place, The Hoe, Plymouth PL1 3DH, UK*
[3]*National Centre for Earth Observations, Plymouth Marine Laboratory, Prospect Place, The Hoe, Plymouth PL1 3DH, UK*

**Corresponding author: tel: +385 99 735 33 55; e-mail: zkovac@pmfst.hr.*

Kovač, Ž., Platt, T., and Sathyendranath, S. Stability and resilience in a nutrient-phytoplankton marine ecosystem model. – ICES Journal of Marine Science, 77: 1556–1572.

Received 25 September 2019; revised 25 February 2020; accepted 10 March 2020; advance access publication 29 June 2020.

We seek to understand, in mathematical terms, the causes of stability in marine phytoplankton biomass. The stability of a simple, mixed-layer-phytoplankton-nutrient model is analysed. Primary production is modelled as a non-linear function of nutrient concentration and light. The steady state of the model system is demonstrated to be stable with a linear relation between steady state biomass and nutrients. The causes of stability are shown to be shading and nutrient limitation. When only light limitation and shading are taken into account, the steady state is a sink node. However, when nutrient limitation is taken into account, without shading, the steady state can be either a sink node or a spiral sink. The transition from a sink node to a spiral sink occurs when normalized mixed layer production becomes larger than the equivalent influx rate of nutrients into the mixed layer, demonstrating that nutrient limitation of production is a necessary, but not a sufficient condition for oscillatory solutions. In both cases, the characteristic return times are derived explicitly. The effect of shading is found to cause the depression of the steady state towards lower biomass than would otherwise be attainable. The influence of mixed-layer depth variation on stability is also analysed.

Keywords: bio-optical control, nutrient phytoplankton model, stability analysis, steady-state resilience

Introduction

In biomass terms, marine phytoplankton form <1% of the total plant biomass on Earth (Bar-On *et al.*, 2018), yet on the annual time scale phytoplankton primary production is commensurate with that of terrestrial plants (Field, 1998; Prentice *et al.*, 2001), converging on 40–50 Gt C per annum (Buitenhuis *et al.*, 2013; Bouman *et al.*, 2018; Kulk *et al.*, 2020). The apparent inconsistency is possible because of the rapid turnover time of phytoplankton, being on the order of days, in comparison with the turnover time of land plants, which may be on the order of weeks to years. Notwithstanding their high turnover times, stable marine phytoplankton assemblages are persistent and stable (Falkowski and Raven, 2007). One manifestation of this stability is the recurring seasonal cycle of phytoplankton abundance (phenology) that is a characteristic of pelagic ecosystems in different oceanic regimes (Platt and Sathyendranath, 2008; Platt *et al.*, 2009).

The advent of data on visible spectral radiometry (ocean colour) of the sea, collected by instruments in Earth's orbit, has provided us with a global picture of phytoplankton abundance, indexed by the surface chlorophyll field at high spatial resolution (≈1 km), and its evolution through time with a nominal resolution of 1 d (Platt *et al.*, 1995). From such imagery we learn that, for most of the time, despite the potentially rapid growth of phytoplankton, the surface chlorophyll field generally changes little from 1 d to the next (Zhai *et al.* 2010). The explanation must be

© International Council for the Exploration of the Sea 2020. All rights reserved.
For permissions, please email: journals.permissions@oup.com

Downloaded from https://academic.oup.com/icesjms/article/77/4/1556/5864492 by guest on 31 December 2021

that stabilizing tendencies exist, which can normally maintain a balance between phytoplankton growth and losses, probably mediated through the principal controls on photosynthesis, namely light and nutrients (Platt *et al.*, 2003a, b). Only rarely do we find that the balance is altered on longer time scales (annual), but we do frequently find significant net growth (or loss) leading to a bloom (or its demise) on shorter time scales (weekly).

There are societal implications entangled with the question of stability of marine ecosystems (Cinner and Barnes, 2019). In legal documents relating to ecosystem-based management of marine resources, the management goals include preservation of ecosystem health, vigour, and resilience. Such properties are not easy to translate into objective metrics that could be applied in operational mode. However, we must try to develop objective metrics, if we are serious about ecosystem-based management. One most tractable property seems to be resilience (Holling, 1996). We understand resilience to imply the operation of stabilizing processes that dampen fluctuations in chlorophyll rather than letting them grow. It is clearly related to the stabilizing tendencies that lie behind the observed conservatism in the surface chlorophyll field of the ocean.

Such considerations suggest that, to crystallize our ideas about phytoplankton resilience, we should study the stability properties of the equations that describe phytoplankton dynamics. Here, we analyse the stability of a simple phytoplankton-nutrient model to elucidate the mechanisms by which fluctuations in chlorophyll can be damped, and the relative speed by which a new steady state can be reached. We limit our considerations to the nutrient-phytoplankton system, without considering explicit details of zooplankton dynamics at this stage. Inclusion of zooplankton changes the dynamical picture by lifting the model from two to three dimensions where more complex trajectories can emerge. Although zooplankton grazing and natural mortality may also play a stabilizing role in chlorophyll fluctuations, we do not consider these processes explicitly, since they have been studied extensively in the literature (Armstrong, 1994; Edwards *et al.*, 1996, 2000; Gibson *et al.*, 2005; Everett *et al.*, 2017).

Matherial and methods

Mixed-layer production

Let the z (m) axis be positive downwards with the origin at the ocean surface (Figure 1) and let day length (time from sunrise till sunset) be given as D (h). Let us consider a mixed layer extending from the surface to Z_m (mixed-layer base), taking Z_m constant for now. Following Platt *et al.* (2003a), we take chlorophyll concentration B (mg Chl m^{-3}) as the index for phytoplankton biomass and nitrogen concentration N (mg N m^{-3}) as a measure of nutrient availability. Downwelling irradiance I (W m^{-2}) at depth serves as a measure of available light for photosynthesis (Platt *et al.*, 1990).

We consider a model where primary production per unit biomass P^B [mg C (mg Chl h)$^{-1}$] is given as a function of light and nutrients $P^B = P^B(I, N)$, where light is a function of depth $I = I(z, t')$ with nutrients uniform over the depth of the mixed layer (i.e. they are not uniform in time), making $P^B = P^B(I(z, t'), N)$. We use the notation t' for time during sun hours (sunrise till sunset). Production is then expressed as a product of a light limiting function and a nutrient limiting function:

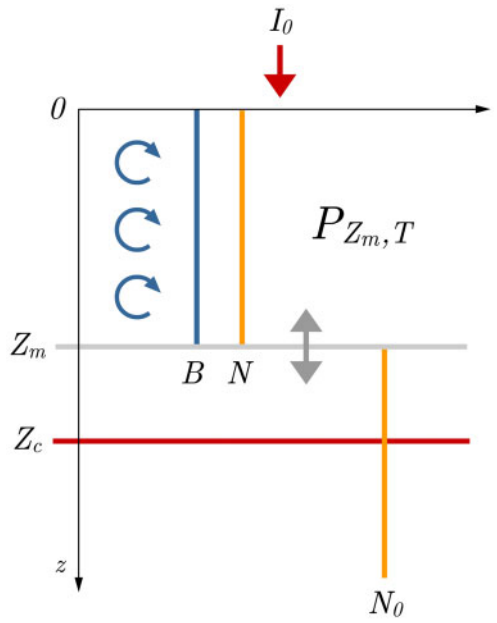

Figure 1. A mixed layer of depth Z_m (grey) with biomass B (blue) and nutrient concentration N (orange), exposed to sinusoidally varying solar irradiance with noon irradiance I_0^m. Green circles indicate mixing. Below the mixed layer, nutrient concentration is N_0 and biomass is assumed zero. Mixed-layer production $P_{Z_m,T}$ (notation following Platt *et al.* (1990)) is fuelled by light downwelling from the surface and the nutrient flux from below the mixed layer. The critical depth where vertically integrated production equals losses is marked Z_c (red line).

$$P^B(N, z, t') = P^B_{\max} \frac{N}{N + N_k} \left[1 - \exp\left(-I(z, t')/I_k\right)\right],$$

where nutrient limitation of production is modelled with the Monod function (Monod, 1949), also known as the Michaelis–Menten function (Michealis and Menten, 1913; Johnson and Goody, 2011), and light limitation with the exponential light saturation function (Platt *et al.*, 1980), having $P^B_{\max}$ as the maximum photosynthetic capacity (Platt and Jassby, 1976), N_k as the half-saturation constant for nutrient limitation (Eppley *et al.*, 1969) and I_k as the photoadaptation parameter (Platt *et al.*, 1980). Typical values of the mentioned parameters, and their units, are given in Table 1.

In the mixed layer, light is a function of depth, whereas nutrient concentration is not, given that mixing is assumed to distribute nutrients evenly in the mixed layer. Biomass remains uniform in the mixed layer for the same reason. We also assume that the time scale of mixing is shorter than the time scale of photoadaptation, meaning there is no variation in I_k over depth (Lewis *et al.*, 1984). Now, daily mixed-layer production is the integral of $B\,P^B(z, t')$ over the mixed layer and day length (Platt *et al.*, 1990; Kovač *et al.*, 2017a):

$$P_{Z_m,T} = B \int_0^D \int_0^{Z_m} P^B(z, t') \mathrm{d}z \mathrm{d}t', \qquad (2)$$

where t' is a dummy variable for integration over day length. To evaluate this integral, we need also to adopt a functional form for $I(z, t')$. First, we assume that during the course of 1 d the mixed layer is exposed to sinusoidally varying surface irradiance, with

Downloaded from https://academic.oup.com/icesjms/article/77/4/1556/5864492 by guest on 31 December 2021

Table 1. Parameters and their values used in the application section.

Parameter	Symbol	Value
Surface noon irradiance	I_0^m	350 W m^{-2}
Attenuation coefficient due to water	K_w	0.04 m^{-1}
Specific attenuation by chlorophyll	k_B	0.015 m^2 (mg Chl)$^{-1}$
Photoadaptation parameter	I_k	40 W m^{-2}
Maximum photosynthetic capacity	$P^B_{\max}$	10 mg C (mg Chl h)$^{-1}$
Loss rate	L^B	0.15 h^{-1}
Mixed-layer depth	Z_m	100 m
Nutrient supply parameter[a]	ξ	0.00025 h^{-1}
Half-saturation constant for nutrient limitation	N_k	5 mg N m^{-3}
Deep nutrient concentration	N_0	50 mg N m^{-3}
Carbon-to-chlorophyll ratio	χ	100 mg C (mg Chl)$^{-1}$
Nitrogen-to-chlorophyll ratio	ν	8 mg N (mg Chl)$^{-1}$

The parameter values are taken from Platt *et al.* (1990, 2003b) and Kovač *et al.* (2016b, 2018b).
[a]See Appendix 1 for interpretation of ξ.

noon irradiance I_0^m. Second, we assume surface irradiance is attenuated with depth by sea water and phytoplankton following Lambert–Beer's law (Kirk, 2011), with the attenuation coefficients K_w and k_BB, respectively, where k_B is the specific attenuation coefficient of phytoplankton. Therefore, for light at depth we have:

$$I(z,t) = I_0^m \sin(2\pi t'/D) \exp(-(K_w + k_BB)z). \tag{3}$$

With these assumptions, daily mixed-layer production $P_{Z_m,T}$ is given as:

$$P_{Z_m,T} = \frac{N}{N+N_k}\frac{BP^B_{\max}D}{K_w+k_BB}\left[f(I_*^m) - f(I_*^m e^{-(K_w+k_BB)Z_m})\right], \tag{4}$$

where $I_*^m = I_0^m/I_k$ is the normalized noon irradiance and $f(I_*^m)$ is a known function:

$$f(I_*^m) = \sum_{n=1}^{\infty} \frac{2(I_*^m)^{2n-1}}{\pi(2n-1)(2n-1)!}\frac{(2n-2)!!}{(2n-1)!!} - \sum_{n=1}^{\infty}\frac{(I_*^m)^{2n}}{2n(2n)!}\frac{(2n-1)!!}{(2n)!!}, \tag{5}$$

as derived by Platt *et al.* (1990). Formulated as such, mixed-layer production is limited by both light and nutrients. Note that light attenuation due to biomass itself is taken into account explicitly, being expressed as a separate (additive) component of the total diffuse attenuation coefficient in the denominator and also in the final term of (4).

Biomass and nutrient dynamics

Let us allow biomass and nutrient concentrations to change over time, making $B(t)$ and $N(t)$ functions of t (h). Time t is a continuous variable and is not associated with the time of day as in the previous section. We model the temporal evolution of biomass with the following equation:

$$\frac{dB(t)}{dt} = \langle P\rangle_{Z_m,T} - L^BB(t), \tag{6}$$

where $\langle P\rangle_{Z_m,T} = P_{Z_m,T}/(24\chi Z_m)$ is the daily average mixed-layer production, per unit volume, scaled by the carbon-to-chlorophyll ratio χ (in other words, in chlorophyll units) and L^B is a generalized loss term including various (negative) contributions to the realized rate of increase in the broadest sense (arising from respiration, grazing, sinking, predation, and mortality; Zhai *et al.*, 2010). Likewise, $\langle P^B\rangle_{Z_m,T} = P_{Z_m,T}/(24\chi Z_mB)$ is the daily average, chlorophyll-specific production in the mixed layer. It is understood that production changes as a function of $B(t)$ and $N(t)$. Biomass below the mixed layer is taken to be zero, the result of unfavourable growth conditions arising from diminished light and/or increased losses; and is therefore not modelled explicitly. This is common practice in modelling mixed-layer biomass dynamics (Huisman and Weissing, 1995; Platt *et al.*, 2003a).

Temporal evolution of nutrient concentration is given by the following equation:

$$\frac{dN(t)}{dt} = -\nu\langle P\rangle_{Z_m,T} + \xi(N_0 - N(t)), \tag{7}$$

and is coupled to the biomass equation via the production term, where ν is the nutrient-to-chlorophyll ratio. Nutrient concentration below the mixed layer is fixed at N_0, representing the deep-water nutrient pool. Influx of nutrients into the mixed layer is modelled by the $\xi(N_0 - N(t))$ term, which can be considered as restorative, pushing the nutrient concentration towards a fixed value N_0 (Huisman and Weissing, 1995). Interpretation of ξ is provided in Appendix 1. We refer to ξ as the nutrient supply parameter. Diminution of nutrients occurs as a consequence of phytoplankton uptake during growth.

For clarity, when fully expanded, the equation for biomass is:

$$\frac{dB(t)}{dt} = \frac{1}{24\chi Z_m}\frac{N}{N+N_k}\frac{BP^B_{\max}D}{K_w+k_BB} \times \left[f(I_0^m/I_k) - f(I_0^m e^{-(K_w+k_BB)Z_m}/I_k)\right] - L^BB(t), \tag{8}$$

and the equation for nutrients is:

$$\frac{dN(t)}{dt} = -\frac{\nu}{24\chi Z_m}\frac{N}{N+N_k}\frac{BP^B_{\max}D}{K_w+k_BB} \times \left[f(I_0^m/I_k) - f(I_0^m e^{-(K_w+k_BB)Z_m}/I_k)\right] + \xi(N_0 - N(t)). \tag{9}$$

Downloaded from https://academic.oup.com/icesjms/article/77/4/1556/5864492 by guest on 31 December 2021

Strictly speaking, these equations describe instantaneous changes in biomass and nutrient concentrations in the mixed layer. For simplicity, in the rest of the paper, we will use the shorter notation as in (6) and (7).

Results

Steady state

The model presented has only two time-dependent prognostic variables, namely $B(t)$ and $N(t)$, allowing us to visualize model behaviour easily in the phase plane (Figure 2), a plane spanned by N and B, such that each point in this plane represents a model state (Perko, 2001). In this work, we place the nutrient concentration on the abscissa and the chlorophyll concentration on the ordinate, for consistency with previous works on the phytoplankton-nutrient system (Huisman and Weissing, 1995; Huppert *et al.*, 2002). The parameters D, Z_m, and I_0^m are here being considered as fixed parameters, even though in reality they vary through time.

A set of points starting from the initial state and evolving in time according to (6) and (7) gives the model trajectory, also referred to as its orbit (Izhikevich, 2007). A set of points for which one variable stops evolving in time is referred to as a nullcline (Truscott and Brindley, 1994) and this model has two nullclines, namely the biomass and the nutrient nullcline (Huisman and Weissing, 1995), each solved separately by setting (6) and (7) equal to 0. The point for which both variables stop changing in time is referred to as the steady state (or fixed point; Robinson, 1995) and it is found at the crossing of the two nullclines. The model also has a trivial nullcline $B=0$ associated with the steady state $(0, N_0)$. This is, however, not the subject of the presented work and the focus is on states with $B>0$.

On the phase plane, the nutrient nullcline is seen to intersect the nutrient axis at N_0 and becomes parallel to the biomass axis with increasing biomass (orange curve in Figure 2), indicating that nutrients are never fully depleted from the mixed layer as biomass increases. This is due to nutrient limitation of production in (1). The biomass nullcline is an increasing function of N with more nutrients supporting more biomass (blue curve in Figure 1). As biomass increases, light limitation of production occurs and biomass levels off for high values of N (Huisman and Weissing, 1995).

For the two nullclines to intersect, the deep-water nutrient concentration N_0 has to exceed a value N_c (Figure 2), which is the critical nutrient concentration required to sustain the population:

$$\frac{1}{24\chi Z_m}\frac{N_c}{N_c+N_k}\frac{P^B_{\max}D}{K_w}\left[f(I^m_*)-f(I^m_* e^{-K_w Z_m})\right]=L^B, \tag{10}$$

from which we get N_c explicitly as:

$$N_c=\frac{N_k}{P^B_{\max}D[f(I^m_*)-f(I^m_* e^{-K_w Z_m})]/(24\chi Z_m L^B K_w)-1}. \tag{11}$$

This is recognized as the point at which the biomass nullcline crosses the N axis (blue point in Figure 2) and is obtained in the limit of $B\to 0$. The steady state corresponding to $N_c > N_0$ is in fact $(0, N_0)$, in other words, the deep-water nutrient concentration is insufficient to sustain any biomass in the mixed layer through vertical transport of nutrients into the mixed layer. The nullclines do not cross in this case. When $N_c < N_0$, the nullclines cross and a steady state $S=(B^*, N^*)$ is obtainable (red point in Figure 2), with both nutrient and biomass different from zero (Huisman and Weissing, 1995). In this case, the deep-water nutrient concentration is sufficient to sustain mixed-layer production and the corresponding biomass. This is a non-trivial equilibrium, and it is the focus of our investigation.

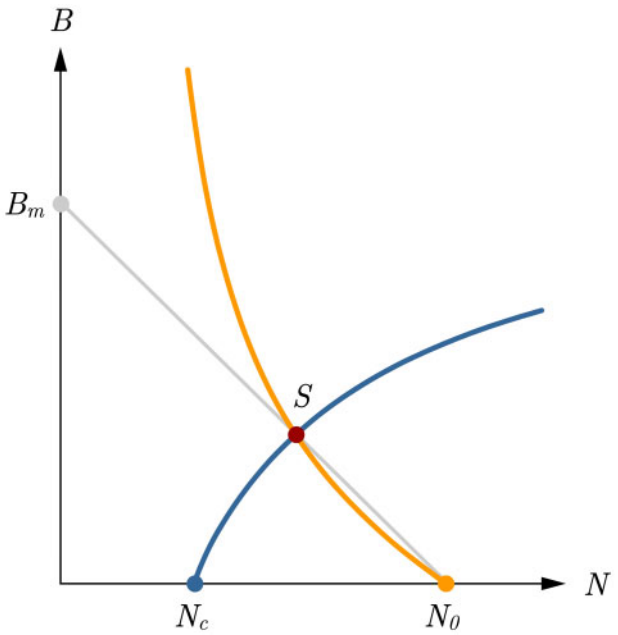

Figure 2. Phase plot of system nullclines: blue curve is the biomass nullcline and the orange curve is the nutrient nullcline. Nutrient nullcline intersects the N axis at N_0 and the biomass nullcline at N_c. For $N_c < N_0$ the two nullclines intersect at the steady state S (red dot). The grey line (termed the steady-state line) marks the conditions that steady state satisfies, termed the steady-state line and gives the steady-state biomass B^* in relation to the difference between the steady-state nutrient concentration in the mixed layer N^* and the deep-water nutrient concentration N_0 (12). Theoretically, B_m (14) is the maximum attainable biomass in case all the nutrients get exhausted, but is never reached due to other constraints of the model.

To find a relation between the steady-state biomass and nutrient concentration, we first multiply (6) by ν, put $\mathrm{d}B(t)/\mathrm{d}t=0$, add to (7), set $\mathrm{d}N(t)/\mathrm{d}t=0$ and rearrange to get:

$$B^*=\frac{\xi}{\nu L^B}(N_0-N^*), \tag{12}$$

as the expression for the steady-state biomass B^* in relation to the difference between the steady-state nutrient concentration in the mixed layer N^* and the deep-water nutrient concentration N_0 (grey line in Figure 2). In the phase plane, we refer to this line as the steady-state line upon which steady states with $B>0$ must lie. Recognizing that at steady state, we have $\langle P^B\rangle_{Z_m,T}=L^B$ we can rewrite the previous expression as:

$$B^*=\frac{\xi}{\nu\langle P^B\rangle_{Z_m,T}}(N_0-N^*). \tag{13}$$

Equations (12) and (13) show how the steady states $B^*>0$ are related to the nutrient supply rate $\xi(N_0-N^*)$ and to the average,

Downloaded from https://academic.oup.com/icesjms/article/77/4/1556/5864492 by guest on 31 December 2021

chlorophyll-specific production in the mixed layer $\langle P^B \rangle_{Z_m,T}$, which itself is also dependent in a non-linear way on both B^* and N^*. A higher nutrient supply parameter ξ makes the steady-state line steeper, therefore, favouring a state with higher biomass relative to nutrient concentration. On the other hand, a lower nutrient supply parameter ξ makes the steady-state line less steep, therefore, favouring a low biomass state relative to nutrient concentration. The exact steady state is naturally set by all the parameters, as all together they determine where the two nullclines will intersect each other and the steady-state line. Also, expression (13) is consistent with observations in the field of an inverse relation between the production per unit biomass and total biomass (Harris, 1984). It provides a theoretical basis for explaining such observations.

The steady-state line passes through the N_0 point on the N axis, which is the maximum possible nutrient concentration in the mixed layer, and is of course set by the deep-water nutrient concentration. According to (12), we see that if there is to be a state with $B^* > 0$ then N^* has to be less than N_0, implying that in case of $N_c < N_0$ (i.e. a non-trivial equilibrium) nutrient concentration never reaches N_0. Also, the steady-state line intersects the biomass axis, thereby setting a limit on the maximum attainable biomass in case all nutrients in the mixed layer were to be utilized (grey point in Figure 2). When N approaches zero, as would be expected towards the end of a bloom, biomass approaches the maximum possible steady-state value B_m given as:

$$B_m = \frac{\xi}{\nu L^B} N_0. \tag{14}$$

To increase this maximum biomass, either the supply rate ξN_0 has to be increased, or the product of ν and L^B reduced. However, because the nutrient nullcline does not intersect the biomass axis, the steady state with this biomass is never reached.

Stability of the steady state

To analyse the stability of the steady state, we linearize the model at steady state and use the Jacobian matrix **J** (Ryabchenko *et al.*, 1997; Kuznetsov, 2004):

$$\mathbf{J} = \begin{bmatrix} \partial_B \langle P \rangle_{Z_m,T} - L^B & \partial_N \langle P \rangle_{Z_m,T} \\ -\nu \partial_B \langle P \rangle_{Z_m,T} & -\nu \partial_N \langle P \rangle_{Z_m,T} - \xi \end{bmatrix}. \tag{15}$$

The Jacobian is fundamental to system stability (Hayking, 2005); for the steady state to be stable it is required that its trace Tr**J** be negative and its determinant det**J** positive (Izhikevich, 2007) (Appendix 2):

$$\mathrm{Tr}\mathbf{J} < 0, \quad \det\mathbf{J} > 0, \tag{16}$$

with Tr**J** equal to:

$$\mathrm{Tr}\mathbf{J} = \partial_B \langle P \rangle_{Z_m,T} - L^B - \nu \partial_N \langle P \rangle_{Z_m,T} - \xi, \tag{17}$$

and det**J** equal to:

$$\det\mathbf{J} = (\partial_B \langle P \rangle_{Z_m,T} - L^B)(-\nu \partial_N \langle P \rangle_{Z_m,T} - \xi) + \nu \partial_B \langle P \rangle_{Z_m,T} \partial_N \langle P \rangle_{Z_m,T}. \tag{18}$$

To explore the sign of the trace, we first use the definition of average mixed-layer production defined using the production profile from Kovač *et al.* (2016a), scaled by χ:

$$\langle P \rangle_{Z_m,T} = \frac{1}{24\chi Z_m} \int_0^{Z_m} B(z) P_T^B(z) \mathrm{d}z = B \langle P^B \rangle_{Z_m,T}, \tag{19}$$

where we have used the homogeneity in biomass $B(z) = B$ to put the biomass B outside the integral and employed the notation $\langle P^B \rangle_{Z_m,T} = P_{Z_m,T}/(24\chi Z_m B)$ for the daily average, specific turnover rate of biomass in the mixed layer. Taking the derivative of the previous expression with respect to biomass gives:

$$\partial_B \langle P \rangle_{Z_m,T} = \langle P^B \rangle_{Z_m,T} + B \partial_B \langle P^B \rangle_{Z_m,T}. \tag{20}$$

Putting this derivative in the expression for the trace and acknowledging that at steady-state production equals losses $\langle P^B \rangle_{Z_m,T} = L^B$ leaves us with a new expression for the trace:

$$\mathrm{Tr}\mathbf{J} = B^* \partial_B \langle P^B \rangle_{Z_m,T} - \nu \partial_N \langle P \rangle_{Z_m,T} - \xi. \tag{21}$$

For the first term in this expression to be smaller than zero it is required that:

$$\partial_B \langle P^B \rangle_{Z_m,T} < 0, \tag{22}$$

which is indeed the case following (3). The intuitive interpretation is that an increase in biomass reduces light intensity at depth and consequently lowers biomass normalized production. This is the meaning of phytoplankton shading, which in the model is expressed by the $k_B B$ term in the attenuation coefficient. Without this term, the previous expression reduces to $\partial_B \langle P^B \rangle_{Z_m,T} = 0$. The second term in the trace is $\nu \partial_N \langle P \rangle_{Z_m,T}$, where ν is a positive constant and the derivative with respect to N, written out explicitly, is:

$$\partial_N \langle P \rangle_{Z_m,T} = \frac{N_k}{N(N+N_k)} \langle P \rangle_{Z_m,T}, \tag{23}$$

which is positive for $N > 0$. The third term in the trace is ξ, positive by definition. Considering that the first term in the trace (21) is negative and the other two terms are positive, with a minus sign, the trace is negative. Therefore, having any of these three processes in the model makes the trace less than zero, meeting the first stability condition (16). The different dynamical processes and their influence on system stability are thus distinguished clearly. The first term arises from shading by phytoplankton, the second from nutrient limitation of production, and the third is related to the vertical nutrient flux into the mixed layer.

Let us now explore the sign of the determinant. Fully expanding expression (18), while acknowledging (20), gives:

$$\det\mathbf{J} = -\xi B^* \partial_B \langle P^B \rangle_{Z_m,T} + \nu \langle P^B \rangle_{Z_m,T} \partial_N \langle P \rangle_{Z_m,T}, \tag{24}$$

which is positive. The determinant being positive, in combination with a negative trace, renders the system stable. These conditions are elaborated in more detail in Appendix 2.

Downloaded from https://academic.oup.com/icesjms/article/77/4/1556/5864492 by guest on 31 December 2021

Resilience of the steady state

The steady state is stable, but there are distinct types of stability with respect to the way the steady state is approached dynamically after being perturbed (Izhikevich, 2007). It is here that resilience can be precisely defined and linked to the eigenvalues of the Jacobian. We adhere to the definition of resilience as the speed of recovery of the system after perturbation following pioneers in ecological resilience (Pimm, 1984; Tilman and Downing, 1994; Holling, 1996). A concept closely related to resilience is the characteristic return time, which is the time required for the initial perturbation to be reduced to its e folding magnitude (Brauer, 1979; Pimm, 1984), and it is the reciprocal of resilience.

In our analysis, we assume that the system finds itself at steady state and the perturbation comes in the form of a disturbance that is not strong enough to alter the description of system dynamics as provided by the Jacobian. In plain terms, we consider the linearized system to provide an adequate description of conditions around the steady state. The way the steady state is reached is determined by an additional condition that sets apart two distinct types of stability that the steady state can exhibit (Izhikevich, 2007). If the following condition is met:

$$(\mathrm{Tr}\,\mathbf{J})^2 - 4\mathrm{det}\mathbf{J} < 0, \tag{25}$$

the steady state will be a spiral sink, whereas if:

$$(\mathrm{Tr}\,\mathbf{J})^2 - 4\mathrm{det}\mathbf{J} > 0, \tag{26}$$

it will be a sink node (see Appendix 2). In the former case, the system exhibits oscillations as it approaches the steady state, whereas in the latter case it does not. When oscillating, the system overshoots the steady state prior to reaching it, whereas when it does not oscillate it does not overshoot, but goes directly to the steady state.

The role of shading

To find the cause of possible oscillatory behaviour, we explore whether condition (25) will be met when only one process is accounted for, either shading or nutrient limitation. For no nutrient limitation, condition (25) reduces to:

$$(B^*\partial_B\langle P^B\rangle_{Z_m,T} + \xi)^2 < 0. \tag{27}$$

Because all the terms in the parentheses are real the above condition is clearly not met. The steady state in this case is a sink node, implying that a model with only shading included, but no nutrient limitation of production, cannot exhibit oscillations around the steady state.

It is interesting to note that in this case the two eigenvalues of the Jacobian are:

$$\lambda_1 = B^*\partial_B\langle P^B\rangle_{Z_m,T} \;\;\&\;\; \lambda_2 = -\xi, \tag{28}$$

both being real and negative, which clearly indicate that the steady state in this regime is stable.

We take these eigenvalues to be quantitative measures of resilience, as they determine the speed of recovery of the system after it is perturbed. They can now be used to ascertain the characteristic return times to the steady state, labelled T_i, where the index i labels the eigenvalues. With the understanding that the characteristic return time is the time required for the initial perturbation to be reduced to its e folding magnitude, by the dynamical response associated with each eigenvalue, we relate T_i to the eigenvalues through $T_i = 1/|\lambda_i|$. The characteristic return times associated with the previous eigenvalues are therefore:

$$T_1 = \frac{1}{B^*|\partial_B\langle P^B\rangle_{Z_m,T}|} \;\;\&\;\; T_2 = \frac{1}{\xi}. \tag{29}$$

The first characteristic return time clearly represents the optical control on the system and the second the role of nutrient flux.

Non-oscillating behaviour on the approach to the steady state was observed by Platt *et al.* (2003a) and Edwards *et al.* (2004) when analysing a coupled biomass nutrient model in which production was not limited by nutrients, except when nutrients were totally depleted. However, it is important to note that their models were discrete in time, whereas the one used here is continuous in time. In the context of the analysis presented here, the reason they did not observe oscillations was simply not having nutrient limitation in the production term in their models. In the next paragraph, we explore how nutrient limitation affects system resilience.

The role of nutrient limitation

We now explore model behaviour when shading is not included in the model, but nutrient limitation of production is. The condition for the steady state to be a spiral sink (25) now reduces to:

$$(\nu\partial_N\langle P\rangle_{Z_m,T})^2 + (2\xi - 4\langle P^B\rangle_{Z_m,T})\nu\partial_N\langle P\rangle_{Z_m,T} + \xi^2 < 0. \tag{30}$$

As a function of $\nu\partial_N\langle P\rangle_{Z_m,T}$, it has a global minimum located at $\nu\partial_N\langle P\rangle_{Z_m,T} = 2\langle P^B\rangle_{Z_m,T} - \xi$. Calculating this function at the aforementioned point, and after some algebra, the previous condition is reduced to:

$$-\langle P^B\rangle^2_{Z_m,T} + \xi\langle P^B\rangle_{Z_m,T} < 0, \tag{31}$$

having a global maximum and two roots, of which one is zero and the other is $\langle P^B\rangle_{Z_m,T} = \xi$. Given that production is by definition positive, we are interested only in the positive root ξ. The previous function is negative for values of $\langle P^B\rangle_{Z_m,T}$ larger than ξ, implying that a necessary condition for a steady state to be a spiral sink is:

$$\langle P^B\rangle_{Z_m,T} > \xi, \tag{32}$$

meaning that the average, specific turnover rate of biomass in the mixed layer needs to be greater than the equivalent nutrient supply parameter for oscillations to occur, i.e. for the steady state to be a spiral sink. As discussed previously, at steady state $\langle P^B\rangle_{Z_m,T} = L^B$, so that the previous expression also translates to:

$$L^B > \xi, \tag{33}$$

meaning that biomass losses have to be larger in magnitude than the nutrient supply parameter for the steady state to be a spiral sink.

The previous expression has implications for nutrient utilization at steady state. Taking the steady-state condition (12) and rearranging it, we get the following ratio:

Downloaded from https://academic.oup.com/icesjms/article/77/4/1556/5864492 by guest on 31 December 2021

$$\frac{\nu B^*}{N_0 - N^*} = \frac{\xi}{L^B}. \tag{34}$$

For steady states that are spiral sinks, L^B is larger than ξ and it follows that the nutrient equivalent of biomass νB^* is less than $N_0 - N^*$. For steady states that are sink nodes, the nutrient equivalent of biomass νB^* is larger than $N_0 - N^*$.

At steady state $\xi(N_0 - N^*)$ is positive, meaning that nutrients flow into the mixed layer at a rate set by ξ. The sink node states also have $\xi > \langle P^B \rangle_{Z_m,T}$, meaning nutrients are being resupplied faster than they are being utilized in primary production, and this is associated with a non-oscillatory behaviour of the steady state. The opposite holds for $\xi < \langle P^B \rangle_{Z_m,T}$ and these states exhibit oscillatory behaviour, nutrients flowing into the mixed layer, at a rate that is insufficient to meet the nutrient demand of primary production.

For these states, which are spiral sinks, the eigenvalues of the Jacobian are a complex conjugate pair (Izhikevich, 2007) with the real part equal to:

$$\mathrm{Re}(\lambda_{1,2}) = \frac{1}{2}\left(-\nu \partial_N \langle P \rangle_{Z_m,T} - \xi\right), \tag{35}$$

which is negative, implying that the system is stable. We now have one characteristic return time:

$$T = \frac{2}{\nu \partial_N \langle P \rangle_{Z_m,T} + \xi}, \tag{36}$$

which is the same for both eigenvalues. In comparison with the characteristic return times associated with the case of no nutrient limitation (29), we observe that the two processes are joined here in the denominator, whereas in (29) each process, shading or nutrient flux, was associated with its own time scale. This means that in case of nutrient limitation and a spiral sink steady state, both nutrient flux and nutrient limitation simultaneously determine the characteristic return time, whereas in case of shading and mixing, two time scales are present, each determined by its own process.

It is interesting to see what happens if and when $\langle P^B \rangle_{Z_m,T} = \xi$. In that case, (30) reduces to:

$$\left(\nu \partial_N \langle P \rangle_{Z_m,T} - \xi\right)^2 < 0, \tag{37}$$

meaning oscillations are excluded. Now the eigenvalues of the steady state are real and distinct from each other:

$$\lambda_1 = -\xi \ \& \ \lambda_2 = -\nu \partial_N \langle P \rangle_{Z_m,T}. \tag{38}$$

with the corresponding characteristic return times:

$$T_1 = \frac{1}{\xi} \ \& \ T_2 = \frac{1}{\nu \partial_N \langle P \rangle_{Z_m,T}}. \tag{39}$$

We see that both eigenvalues are real and negative, meaning that the steady state remains stable. The change of the eigenvalues indicates a change in the type of the steady state, which transitions from a spiral sink to a sink node as $\langle P^B \rangle_{Z_m,T}$ crosses the critical value equal to ξ.

In general, when both processes, shading and nutrient limitation, are modelled together, the characteristic return times can also be found and they are given in Appendix 3.

Bio-optical control of the nullclines

In the previous section, we identified shading as equivalent to a damping mechanism and nutrient limitation of production as equivalent to a damped oscillating mechanism. These two mechanisms work together to reverse a perturbation, such that the system will tend to return once more to steady state. Where exactly in the phase space this steady state will be depends on the crossing of the two nullclines. We know that the biomass nullcline crosses the nutrient axis at N_c and the nutrient nullcline at the steady state S. However, an interesting observation is that in case of no shading, i.e. when $k_B = 0$, it also crosses the nutrient nullcline at N_c (Figure 3).

To demonstrate this, we explore the tangent to the biomass nullcline at steady state S. From (15), and using (20), we have for the slope of the tangent on the biomass nullcline:

$$\left.\frac{\mathrm{d}B}{\mathrm{d}N}\right|_S = -\frac{\partial_N \langle P \rangle_{Z_m,T}}{B^* \partial_B \langle P^B \rangle_{Z_m,T}}. \tag{40}$$

We see that the shading term is in the denominator, therefore the smaller it is, the steeper is the tangent to the biomass nullcline at steady state. For no shading the slope of the tangent is infinite, and for shading included in the model the tangent to the biomass nullcline leans to the right (Figure 3).

Having $k_B = 0$ (no shading) in the model allows us to find an explicit expression for the steady state. Starting with (12) and recognizing that a vertical biomass nullcline crosses the steady-state line at the following point:

$$B^* = \frac{\xi(N_0 - N_c)}{\nu \langle P^B \rangle_{Z_m,T}}, \tag{41}$$

and acknowledging that all steady states lie on the steady-state line, implies that this expression is the steady-state solution for biomass in case of no shading. It is obvious that N_c is the steady-state nutrient concentration in this case. For a model with shading, the steady state will lie in the phase plane to the right and below this steady state (Figure 3).

From our analysis, we see that shading is the reason that the nutrient concentration at steady state exceeds the critical nutrient concentration N_c. Therefore, bio-optical control is responsible for the result that nutrients are not depleted down to the critical nutrient concentration. This occurs because, due to shading, biomass growth is restricted sooner than in the case when only nutrient limitation is in play. With shading, the maximum biomass is reached before nutrients attain the steady-state concentration and highest biomass is not associated with the lowest nutrient concentration. Without shading, more nutrients are exhausted before nutrient limitation steps in, blocking a further increase in biomass.

Mixed-layer depth and stability

In the model equations, mixed-layer depth Z_m appears as a parameter. When it is fixed in time, the model behaves as already

Downloaded from https://academic.oup.com/icesjms/article/77/4/1556/5864492 by guest on 31 December 2021

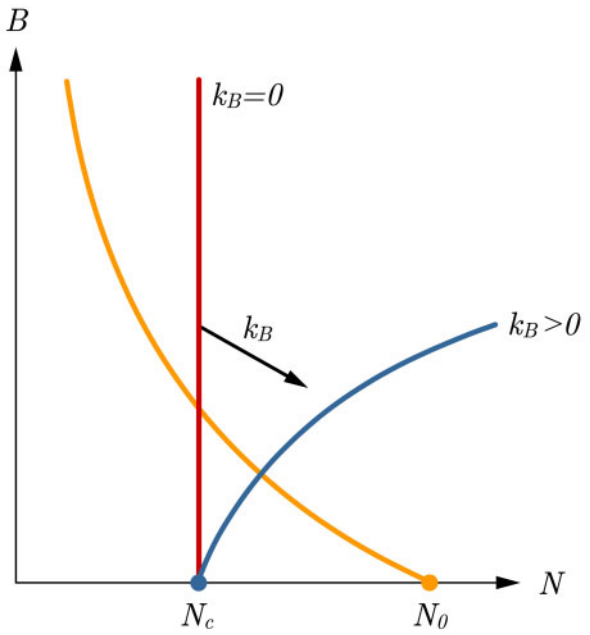

Figure 3. Phase plane sketch of the effect phytoplankton shading has on the slope of the biomass nullcline. For $k_B = 0$ (no shading modelled) the biomass nullcilne is vertical (red line) and for $k_B > 0$ (shading modelled) the biomass nullcline leans to the right (blue curve).

described. However, when Z_m is a function of time, the model is driven not only by initial conditions and the dynamical equations, but also by varying mixed-layer depth. Generally, time dependence of mixed-layer depth can be arbitrary, but for the purpose of stability analysis, we look at intervals of shallowing or deepening separately.

In case of mixed-layer shallowing, the basic model equations (6) and (7) still hold and no additional modifications to the model are required to take into account the effect of shallowing. Therefore, the previous analysis is valid. The only effect that has to be taken into account is the change in average mixed-layer production that occurs as a result of shallowing, and this is implicit in the equations themselves.

However, when mixed layer deepens, nutrients from below the mixed layer are entrained and mixed-layer nutrient concentration increases. The opposite happens with phytoplankton, which becomes diluted, and chlorophyll concentration drops as a consequence of deepening. To model mixed-layer deepening, basic equations (6) and (7) have to be augmented to account for the effect of biomass dilution and nutrient enrichment. The augmented set of equations is given explicitly as (Zhai *et al.*, 2010):

$$\frac{\mathrm{d}B(t)}{\mathrm{d}t} = \langle P\rangle_{Z_m(t),T} - L^B B(t) - \frac{1}{Z_m(t)}\frac{\mathrm{d}Z_m(t)}{\mathrm{d}t}B(t), \tag{42}$$

and:

$$\frac{\mathrm{d}N(t)}{\mathrm{d}t} = -\nu\langle P\rangle_{Z_m(t),T} + \xi(N_0 - N(t)) + \frac{1}{Z_m(t)}\frac{\mathrm{d}Z_m(t)}{\mathrm{d}t}(N_0 - N(t)). \tag{43}$$

We recognize $(1/Z_m)(\mathrm{d}Z_m/\mathrm{d}t)$ as the deepening term. During deepening, biomass losses are effectively increased and nutrient supply from the deep-water nutrient pool is increased. It is clear that such a process will move the system away from steady state. However, we are here interested in how it affects the stability of the system, not the detailed response of the system to deepening.

To study the stability, in this case, we begin by linearizing the above system of equations to obtain the following Jacobian:

$$\mathbf{J} = \begin{bmatrix} \partial_B\langle P\rangle_{Z_m,T} - L^B - \frac{1}{Z_m}\frac{\mathrm{d}Z_m}{\mathrm{d}t} & \partial_N\langle P\rangle_{Z_m,T} \\ -\nu\partial_B\langle P\rangle_{Z_m,T} & -\nu\partial_N\langle P\rangle_{Z_m,T} - \xi - \frac{1}{Z_m}\frac{\mathrm{d}Z_m}{\mathrm{d}t} \end{bmatrix}. \tag{44}$$

In comparison with the original Jacobian (15), we notice the addition of the deepening term $(1/Z_m)(\mathrm{d}Z_m/\mathrm{d}t)$ on the diagonal. As far as the stability of the system is concerned, the addition of the deepening term $(1/Z_m)(\mathrm{d}Z_m/\mathrm{d}t)$ does not change the sign of the determinant, nor that of the trace of the augmented Jacobian (44). Therefore, during deepening the system remains stable.

In this case, let us assume $\xi = 0$. We see from the nutrient equation (43) that in place of ξ we have $(1/Z_m)(\mathrm{d}Z_m/\mathrm{d}t)$, implying that the role of $(1/Z_m)(\mathrm{d}Z_m/\mathrm{d}t)$ is the same as that of ξ with respect to nutrient concentration: both act to increase nutrient concentration in the mixed layer. In a scenario where ξ were indeed small, or non-existent, mixed-layer deepening would serve as the only means of nutrient enrichment.

When the mixed-layer depth changes abruptly, we can look at that change not as a continuous process, but model it as a step change. We look first at the case of shallowing and explore what happens when mixed-layer depth changes at time t_0 in the form of a step function:

$$Z_m = \begin{cases} Z_d & t \le t_0 \\ Z_s & t > t_0 \end{cases}, \tag{45}$$

with $Z_s < Z_d$, where Z_s is the shallow mixed-layer depth and Z_d is the deep mixed-layer depth (Figure 4). As already stated, the governing equations (6) and (7) hold for shallowing. However, to an abrupt change in Z_m the system cannot respond instantaneously, and a dynamic response ensues. Briefly, upon abrupt shallowing, the average mixed-layer production increases (Appendix 4) but the losses do not change, which subsequently causes an imbalance in the biomass and nutrient equations. The system has effectively acquired a new shallow steady state S_s and the previous deep steady state S_d acts as the initial condition for the approach to the new steady state (Figure 4). By the analysis given in the Stability of the steady state section, both states are stable and the system approaches the new steady state. This corresponds to the classical depiction of the spring bloom given by Sverdrup (1953). Complementary to Sverdrup (1953) we now see that, depending on the magnitudes of the model parameters, the approach to the steady state will be either oscillatory or non-oscillatory, as laid out in the Resilience of the steady state section.

When the mixed layer deepens abruptly (Figure 5), we have the following:

$$Z_m = \begin{cases} Z_s & t \le t_0 \\ Z_d & t > t_0 \end{cases}, \tag{46}$$

Downloaded from https://academic.oup.com/icesjms/article/77/4/1556/5864492 by guest on 31 December 2021

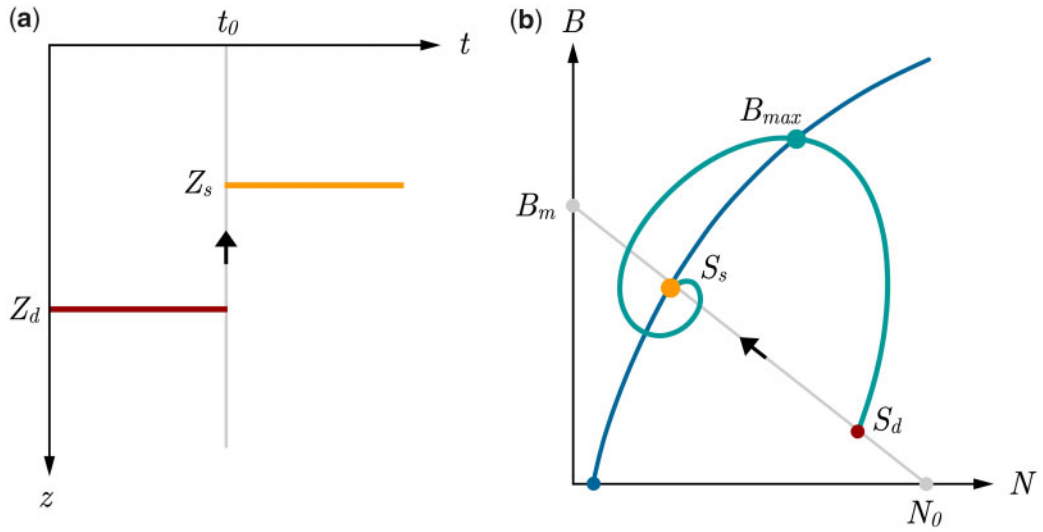

Figure 4. Sketch of the model response to abrupt mixed-layer shallowing. (a) Mixed-layer depth as a function of time. The system starts with mixed-layer depth Z_d and at time t_0 abruptly shallows to the depth Z_s. (b) The change of steady states as seen in the phase space. As the mixed layer shallows, the system goes from the state S_d (red point) to the state S_s (orange point). Both states lie on the steady-state line (12). The maximum biomass B_{max} reached on the approach to S_s is located at the crossing of the biomass nullcline (blue curve) and the trajectory (green curve).

In this case, biomass is diluted due to deepening and nutrient concentration increases due to entrainment of the deep-water nutrients. Because of deepening the system moves from the steady state S_s to the intermediate state S_i (Figure 5). Total biomass in the mixed layer is conserved during abrupt deepening and biomass at the intermediate state B_i can easily be calculated as:

$$B_i = \frac{Z_s}{Z_d} B_s, \tag{47}$$

whereas nutrient concentration increases due to entrainment and for N_i we have:

$$N_i = N_0 + (N_s - N_0)\frac{Z_s}{Z_d}. \tag{48}$$

From this intermediate state S_i, the system then approaches the newly acquired deep steady state S_d.

The distinction between the case of continuous deepening and the case of abrupt deepening is in the augmentation of equations. If we treat deepening as continuous then (6) and (7) become (42) and (43) during deepening. If we treat deepening as abrupt then (6) and (7) still hold and do not need to be augmented. The way abrupt deepening is taken into account is by the change of state after deepening. So at the moment of deepening t_0, the state of the system goes to S_i (47, 48). Because the equations remain the same, the system remains stable.

Timing of maximum biomass

Given that $B_d < B_s$ after shallowing, biomass is certain to reach its maximum. For a sink node this maximum equals the shallow steady-state biomass B_s and is approached asymptotically. Therefore, it is already known. For a spiral sink, steady-state maximum biomass does not equal the shallow steady-state biomass B_s, as the trajectory can surpass it during the approach to the steady state. Here, we calculate this maximum biomass B_{max} and also the timing of its occurrence t_{max}.

We assume the system finds itself at the deep steady state S_d and then abruptly shallows to the shallow steady state S_s. Upon linearizing the system around S_s we have an approximation to the trajectory around S_s. Using (57) from the Appendix 2, the time evolution of biomass is approximated as:

$$B(t) \approx B_s + c_1 \exp(\lambda_1 t) v_{11} + c_2 \exp(\lambda_2 t) v_{21}. \tag{49}$$

Since the derivative of $B(t)$ with respect to time equals zero when $B(t)$ reaches the maximum, we find the timing of the maximum by solving:

$$\frac{dB(t)}{dt} = 0. \tag{50}$$

Taking the time derivative of (49), equating it with zero, while using (61) in place of the eigenvalues in the exponential functions, and after some algebra, we find:

$$\exp\left(-\sqrt{(\mathrm{Tr}\mathbf{J})^2 - 4\det\mathbf{J}}\, t\right) = -\frac{\lambda_1 c_1 v_{11}}{\lambda_2 c_2 v_{21}}, \tag{51}$$

where λ_1 and λ_2 are the eigenvalues of the Jacobian at S_s, c_1 and c_2 constants based on initial conditions, v_{11} and v_{21} elements of the eigenvectors of the Jacobian at S_s (Appendix 2). From this, we express the timing of the maximum t_{max} as:

$$t_{max} = \frac{\ln(-\lambda_2 c_2 v_{21}/\lambda_1 c_1 v_{11})}{\sqrt{(\mathrm{Tr}\mathbf{J})^2 - 4\det\mathbf{J}}}. \tag{52}$$

Knowing t_{max} we have an approximate expression for B_{max}:

$$B_{max} \approx B_s + + c_1 \exp(\lambda_1 t_{max}) v_{11} + c_2 \exp(\lambda_2 t_{max}) v_{21}. \tag{53}$$

In the phase plane, this corresponds to the trajectory crossing the biomass nullcline. Starting from S_d the trajectory spirals towards S_s. The first crossing of the trajectory and the biomass

Downloaded from https://academic.oup.com/icesjms/article/77/4/1556/5864492 by guest on 31 December 2021

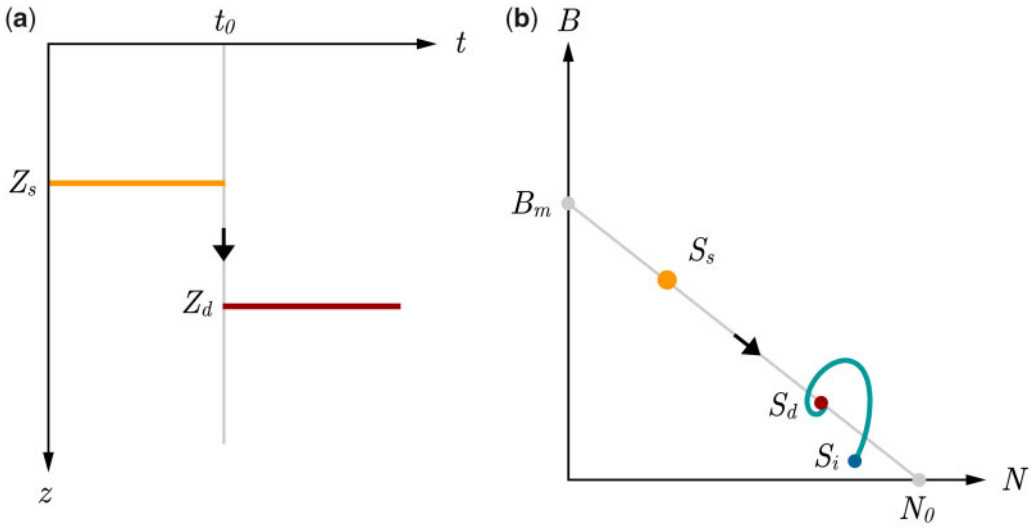

Figure 5. Sketch of the model response to mixed-layer deepening. (a) Mixed-layer depth as a function of time. The system starts with mixed-layer depth Z_s and at time t_0 abruptly shallows to the depth Z_d. (b) The change of steady states as seen in the phase space. As the mixed layer deepens the system goes from the state S_s (orange point) to the intermediate state S_i (blue point). It then starts from S_i to approach S_d (red point).

nullcline corresponds to B_{max}, because due to damping, other crossings occur at lower biomasses.

Application

By equating (6) and (7) with zero, we can solve for B^* and N^* numerically. A plot of the steady-state biomass and nutrients, obtained in such a way, is given in Figure 6c as a function of mixed-layer depth Z_m. When Z_m increases, steady-state biomass declines, whereas steady-state nutrient concentration increases. This is expected as deeper mixed layers have lower average production (Appendix 4) for the same set of parameter values (given in Table 1). According to (12), the steady-state line does not depend on mixed-layer depth. Therefore, with parameters from Table 1, changing the mixed-layer depth will simply move the steady state up and down the steady-state line (Figure 2). Consequently, according to (12), lower steady-state biomass is associated with higher steady-state nutrient concentration and vice versa. This is evident in Figure 6c where B^* and N^* are plotted as functions of Z_m. It is noteworthy that both B^* and N^* vary smoothly with depth, which is not always the case with the characteristic return time, as we now demonstrate.

For each depth, we linearized the system using the obtained steady-state biomass and nutrients for the corresponding depth. Following the procedure outlined in Appendix 3, we calculated the characteristic return time and plotted it as a function of mixed-layer depth Z_m (Figure 6a). Starting from $Z_m = 0$, the characteristic return time has two values (dashed curves), which then merge into one value as mixed-layer depth increases (red curve). This merging corresponds to the change in steady-state type, which transitions from a sink node to a spiral sink as $(\mathrm{Tr}\mathbf{J})^2 - 4\det\mathbf{J}$ becomes negative. In the depth range for which it is a sink node, the steady state has two characteristic return times corresponding to the two eigenvalues (Appendix 2). As mixed-layer depth increases, the eigenvalues change type, becoming complex conjugate. The absolute value of the imaginary part of the eigenvalues is given in Figure 6b (blue curve). From the imaginary part of the eigenvalues, the period of the oscillations can easily be calculated with (64), as demonstrated in Appendix 3. However, here we have plotted the imaginary part directly to emphasize that it becomes distinct from zero at a certain depth. Mixed layers deeper than this depth will behave in an oscillatory manner, whereas shallower ones will not. Therefore we see that mixed-layer depth determines not only whether or not mixed-layer biomass can be sustained (Sverdrup, 1953), but also the character of the dynamical response of the system.

In case of oscillations, we have demonstrated how the timing of the maximum can be found and derived (52). For the example given here we have presented t_{max} as a function of Z_m in Figure 6a (orange curve). In this case, the mixed layer shallows from a depth of 200 m to the depth Z_m, which corresponds to the axis in the figure. Using t_{max}, we have further calculated B_{max} by using (53) and the result is plotted in Figure 6c (dotted green line). At the depth where the steady state switches from a spiral sink to a sink node the maximum biomass drops abruptly, providing a plausible rationale for the well-known phenomenon of the sudden ending, or crash, of blooms by stopping oscillations due to a change in the type of steady state, prior to a total depletion of nutrients. As the state transitions from a spiral sink to a sink node, the initiated oscillatory response, due to shallowing of a deep mixed layer, also terminates. Therefore this transition is of some significance, because it may determine the intensity and duration of the bloom, which have consequences for the rest of the ecosystem. We see that deeper mixed layers can have B_{max} commensurate in magnitude, and even higher, than the steady-state biomass of the shallower layers. These shallower layers, due to their corresponding steady state not being oscillatory, cannot reach such high biomass, even though their steady-state biomass is higher than the steady-state biomass of the deep mixed layers. Thus, we demonstrated the significance of the dynamical view of the phytoplankton-nutrient system.

Downloaded from https://academic.oup.com/icesjms/article/77/4/1556/5864492 by guest on 31 December 2021

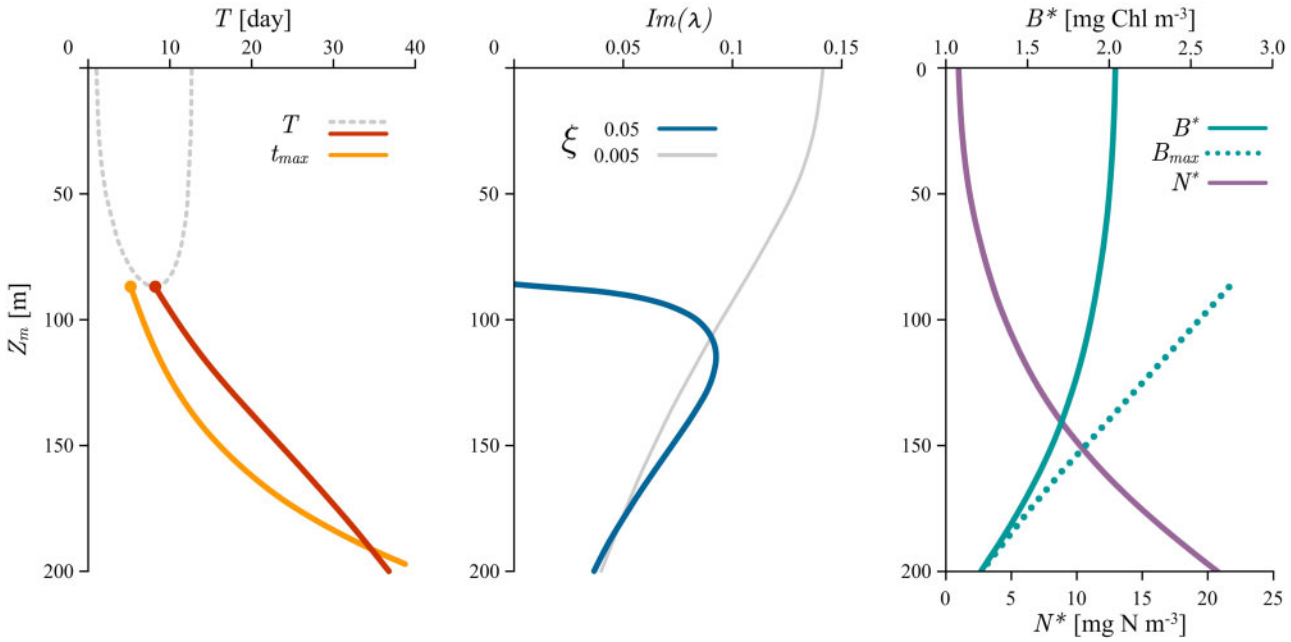

Figure 6. (a) Characteristic return time as a function of mixed-layer depth Z_m (dashed grey and black curves and red curve) and timing of the maximum t_{max} (orange curve) in case of shallowing from 200 m. (b) Absolute value of the imaginary part of the eigenvalues λ_1 and λ_2 for two values of the nutrient supply parameter: $\xi = 0.05\ h^{-1}$ (blue curve) and $\xi = 0.005\ h^{-1}$ (grey curve) as a function of Z_m. (c) Steady-state biomass B^* (green curve) and steady-state nutrient concentration N (purple curve) as a function of Z_m, along with the maximum biomass B_{max} reached in case of shallowing from 200 m (dotted green line).

This discussion can also be cast as an argument based on the nutrient supply rate $\xi(N_0 - N(t))$. We can fix the mixed-layer depth and vary ξ to explore how it affects the eigenvalues and therefore the characteristic return time. An example is given in Figure 7 where the mixed-layer depth is fixed at 100 m and ξ is varied. The characteristic return time is here given as a function of ξ, calculated by following the same procedure as above. The characteristic return time is a smoothly varying function of ξ until, at a particular value of ξ it branches and acquires two distinct characteristic return times. At this point, the imaginary parts of both eigenvalues go to zero.

According to Figure 7, and perhaps contrary to conventional wisdom, mixed layers with a lower nutrient supply parameter behave in an oscillatory manner, whereas the ones with higher nutrient supply rates, and therefore higher nutrient availability, behave in a non-oscillatory manner. This was found to occur as a consequence of the nutrient limitation term in the production model (as described in the Resilience of the steady state section). Without the nutrient limitation term, oscillations cannot emerge, irrespective of the nutrient supply rate. Only when nutrient limitation and supply are both taken into account can oscillations emerge. This leads to the unexpected result that shallower layers, which have higher steady-state biomass, after shallowing, cannot reach biomasses as high as deeper layers can, which have lower steady-state biomass. A simple explanation is that shallower layers can be saturated more easily, that is, the nutrient supply parameter does not have to be as high to cause nutrient saturation of production, as is the case with deeper layers. The same behaviour is seen in Figure 7, but here ξ is varied for a constant mixed-layer depth. As ξ increases, the likelihood of production saturation due to nutrient concentration increases. More on interpretation of ξ is given in Appendix 4.

Discussion

Summary

We have presented a stability analysis of a simple phytoplankton-nutrient model in which primary production is limited by light and nutrient concentration simultaneously. Throughout the paper, historical notation was used and in Appendix 5 we provide a generic version of the model. In previous works of such nature, production limitation was treated in a slightly more simple way, with either light or nutrients limiting production (Huppert *et al.*, 2004, 2005; Platt *et al.*, 2009). As we have demonstrated, nutrient limitation is the primary cause of oscillating behaviour in the model, and light limitation of production is the primary cause of damping. Therefore, in a model with only nutrient limitation, oscillations are damped less quickly in comparison with models having both nutrient and light limitation of primary production. Also, we have shown that shading by phytoplankton itself has a significant effect as it tilts the biomass nullcline to the right in the phase plane (Figure 3) and causes the steady-state biomass to lie below what it would otherwise be in case of no shading. This is not possible in the models of the form studied in Huppert *et al.* (2002), which do not include the effect of shading by phytoplankton and therefore have a vertical biomass nullcline in the phase plane. With respect to temporal evolution, it implies that the peak in biomass occurs sooner than in case of no shading by phytoplankton. Consequently, the timing of the bloom peak is affected. The steady-state biomass attainable in case of no shading was also found, given by (41).

With shading included, we have found an expression relating the steady-state biomass and the steady-state nutrient concentration (12). In phase space it is recognized as the steady-state line (Figure 2). The particular point that is the steady state is

Downloaded from https://academic.oup.com/icesjms/article/77/4/1556/5864492 by guest on 31 December 2021

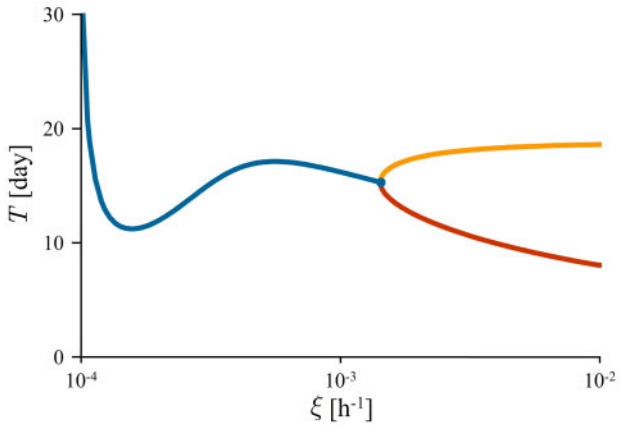

Figure 7. Characteristic return time as a function of ξ. The characteristic return time is a smoothly varying function of ξ (blue curve) until, at a particular value of ξ it branches and acquires two distinct characteristic return times (orange and red curves). In this example, mixed-layer depth Z_m is fixed at 100 m.

determined by the crossing of the nullclines, and it depends on the parameters of the system. A change in the parameters can be viewed as causing a change in the steady state and the dynamical response arises from the system's being attracted to the new steady state. The approach to the steady state is fuelled by nutrients from below and energized by light emanating from the surface. Without additional perturbations, the system very rapidly goes to this new steady state. In fact, the speed of recovery is on the order of the characteristic return time. However, if the perturbations to the steady state have shorter duration than the characteristic return time we can then expect that the steady state will not be reached at all.

The analysis presented is consistent with general knowledge about the functioning of marine ecosystems, namely mixed-layer shallowing is a mechanism for triggering a dynamical response of the phytoplankton-nutrient system, via an increase in light availability to the phytoplankton in the mixed layer (Appendix 3). Our work added to this the understating of shading and nutrient limitation of production as two different damping mechanisms. For shading, it is clear that as biomass increases, light penetration is reduced and therefore production drops. Any value of biomass above the steady-state concentration will be depressed by shading. This, combined with a linear increase of losses with respect to biomass, finally causes the biomass to decline after reaching a maximum value.

As far as nutrient limitation is concerned, as biomass increases with increased production, nutrients are consumed and nutrient concentration drops. With falling nutrient concentration, nutrient limitation of production intervenes, preventing total exhaustion of nutrients from the mixed layer. A consequence is that as the concentration continues to fall, the gradient between deep-water nutrient concentration and the mixed-layer nutrient concentration increases, which in turn increases the influx of deep-water nutrients into the mixed layer. This helps increase production and move the nutrient concentration towards the steady state value. As the nutrients are resupplied, production again increases and the cycle repeats.

When both processes (shading and nutrient limitation) are modelled together, two distinct responses can emerge, both of which satisfy Sverdrup's critical depth criterion (Sverdrup, 1953). The important distinction between the two responses to mixed-layer shallowing is in the approach to the new steady-state biomass. For a sink node, the biomass does not increase above the new steady-state biomass, whereas for a spiral sink it does. We see that, complementary to Sverdrup's criterion, the type of steady state also determines how high biomass can be attained.

An interesting property of the trajectory for a spiral sink is that, when the steady state is being approached, biomass can reach values well above the steady-state value. For a spiral sink steady state, the trajectory can exhibit several orbits around the steady state before the oscillations are damped significantly. How long these oscillations persist is determined by the characteristic return time and it reflects the resilience of the system. It also has consequences for the convergence of the critical depth to the mixed-layer depth. Specifically, the steady state has a unique property with steady-state mixed-layer production exactly balanced by mixed-layer losses. This can be seen by setting $\mathrm{d}B/\mathrm{d}t = 0$ in (6) to obtain:

$$P^B_{Z_m,T} = 24\chi Z_m L^B. \tag{54}$$

Given that the depth for which this criterion holds is referred to as the critical depth, the two depths Z_m and Z_c are in fact equal for the system in steady state. Since the system trajectory converges onto the steady state, the critical depth also converges onto the mixed-layer depth (Platt *et al.*, 2003a).

After shallowing, steady-state oscillations are excluded for the sink node and the critical depth remains deeper than the mixed-layer depth until the new steady state is reached, at which point they become equal. For the spiral sink steady state, there are oscillations, and the critical depth can cross the mixed-layer depth multiple times on the approach to the new steady state. Every crossing is associated with reversing of the net growth rate sign, which switches from positive to negative as the critical depth becomes shallower than the mixed-layer depth and from negative to positive as the critical depth becomes deeper than the mixed-layer depth. This means that positive and negative growth intervals occur during the transition to the new steady state. As time progresses, these oscillations are damped, but their period does not change; it is determined by the imaginary part of the eigenvalues of the Jacobian at the new steady state (Appendix 5).

In both cases, oscillatory and non-oscillatory, the system responds so as to minimize the effect of the disturbance, the disturbance here being a change in the mixed-layer depth. Since all steady states are characterized by the critical depth's being equal to the mixed-layer depth, during the transition states the critical depth is not equal to the mixed-layer depth. Whenever there is an inequality between the two, biomass and nutrient concentration change with time, in a way that minimizes the difference between the two depths. Following mixed-layer shallowing, for a spiral sink steady state, this difference can be both positive and negative, whereas for a sink node it can only be positive. In this case, the critical depth can only be deeper than the mixed-layer depth. Given that critical depth is deeper during the approach to the new steady state, the biomass increases until the critical depth matches the mixed-layer depth. The net growth phase then terminates. Note that the critical depth does not become shallower than the mixed-layer depth and the biomass does not overshoot the new steady-state biomass. Although the growth rate is positive

Downloaded from https://academic.oup.com/icesjms/article/77/4/1556/5864492 by guest on 31 December 2021

during the entire process, there is no increase in biomass beyond the difference in the biomasses of the two steady states. However, this is not the case with a spiral sink steady state; on the approach to the new steady state the net growth rate changes sign, as already discussed.

Minimizing the depth difference between the mixed-layer depth and the critical depth could be a principle valid not only for perturbations caused by variations in the mixed-layer depth, but also for other perturbations, such as a change in surface irradiance, or in the loss rate. A change in surface irradiance arises naturally from cloud coverage and the evolution of the seasons. A change in the loss rate comes naturally from fluctuations in zooplankton abundance, naturally dependent on phytoplankton concentrations, which changes grazing intensity (Edwards and Yool, 2000; Edwards and Bees, 2001). Another way that zooplankton abundance might change is by fishing (Wiborg, 1976), a radical example of which would be exploitation of zooplankton, which might then greatly reduce the phytoplankton loss term and so act as a perturbation on the system. For example, zooplankton have been exploited off the Norwegian coast at least since 1960 (Wiborg, 1976), and has recently increased such that the total allowable catch for 2019 was set at 250 000 tonnes (target species, the copepod *Calanus finmarchicus*). Some ten licences have been issued without specific vessel quota, with a lifetime up to 2029 (fiskerforum.com/norway-sees-commercial-fishery-in-copepods/). Previously, one company had been operating on a trial basis with a modest quota of 5000 tonnes. The potential impact of a 50-fold increase in quota remains to be seen. However, zooplankton dynamics are not modelled explicitly here; zooplankton exploitation would be included implicitly as a reductive contribution to the generalized loss term $-L^B B$ in the phytoplankton equation (6). Adding an additional explicit equation for zooplankton and exploring system stability in that case is a potential course for future research and could be used to study theoretically the effect of zooplankton on the characteristic return times.

Another potential usage of the presented analysis deals with the incorporation of the equations into more complex ecosystem models, nowadays routinely done by modellers. In this context the governing equations can be regarded as a finite volume balances for particular boxes. The production and losses of phytoplankton, along with nutrient uptake, are called the reaction terms of these models. The one term remaining is the $\xi(N_0 - N(t))$ term, which is basically the flux from neighbouring cells. In a three dimensional ocean ecosystem model this term would have to be extended to include fluxes from the top, left and right, front and back, neighbouring boxes. The analysis carried out in this work could provide stability conditions for each box and would subsequently provide criteria for oscillatory behaviour in the entire model. It would also provide an expected return time, which could then easily be compared with the results of more complex marine ecosystem models. This would provide us with a tool for assessing the influence complexity has on the basic behaviour displayed by the model presented here.

In addition, the flux term from neighbouring boxes would also emerge in the biomass equation. Translated to our case of a mixed layer, the only other box is the one below the mixed layer. We have taken the biomass below the mixed layer as zero, effectively making the biomass influx zero. This is a reasonable first-order assumption commonly used in oceanography. However, it may not always be valid. Taking the biomass below the mixed layer as non-zero would have implications for the loss rate, as the flux due to a gradient in biomass would either increase/decrease the biomass in the mixed layer depending on the sign of the gradient, which would subsequently have consequences for the stability criterion of the system. Exploring this effect in more detail is another potential course for future research.

Conclusions

We have seen that the dynamics of even a simple phytoplankton-nutrient model, for which phytoplankton growth rate is nutrient-dependent, are complex, especially in so far as the stability against perturbation of model parameters is concerned. We have found closed solutions for the return times of the phytoplankton biomass (indexed as chlorophyll concentration) following perturbation of parameters. The return times are proposed as metrics for resilience of the pelagic ecosystem. The return to equilibrium may be oscillatory or not, depending on conditions. Importantly, the oscillatory approach to steady state can affect both the amplitude and phase (timing) of the system response to perturbation. In other words, it can affect the phenology of the phytoplankton, which has been shown to play a major role in the survival of larval fish (Platt *et al.*, 2003b, 2007; Friedland *et al.*, 2008). Key model parameters, the mixed-layer depth and the resupply rate of nutrients from the deep reservoir, can both be expected to change under climate change, with implications for the future resilience of the pelagic ecosystem. For example, in the Adriatic Sea regime shifts have been detected in a 55-year time series of primary production (Kovač *et al.*, 2018a) and it is plausible that resilience also changes with regime shifts.

Another threat to resilience is through manipulation of the loss parameter, for example through commercial exploitation of the zooplankton community. In simple ecosystems with few trophic connections, such as those in high latitudes, heavy exploitation of zooplankton may be sufficient to destabilize the pelagic system, and so should be approached with adherence to the precautionary principle. The model that was chosen for analysis had two variables in the phase plane, with loss term parametrized as a linear portion of biomass. The next step is to include zooplankton as the (explicit) third state variable, which changes the dynamics from two to three dimensions and may cause more complex dynamical behaviour (Strogatz, 1994).

The dynamics studied here, which evolve in response to transient modifications of model parameters, are embedded in a context of seasonal change consequent on time-dependent variation in forcing, notably to progressive changes in insolation and stratification. How variability on the transient or episodic scale can be reconciled with that on the seasonal scale also remains the subject of further study. There is now evidence that transient events, such as hurricanes, which primarily affect the mixed layer, can also enhance export of labile carbon to the deep ocean (Pedrosa-Pamies *et al.*, 2019). The link with even longer time scales and the evidence of a response by the marine ecosystem to climate change say through the demonstration of a trend, might be more elusive than previously supposed. Perhaps, the reason is that the ecosystem has built-in stabilizing or compensating tendencies that might obscure or suppress such trends. The results presented in this work show what these might be like, how strong and how rapid. The interpretation of time series data on chlorophyll concentration, such as those provided by the Ocean-Colour Climate-Change Initiative of the European Space Agency (Sathyendranath *et al.*, 2019), will become more complex as a result.

Downloaded from https://academic.oup.com/icesjms/article/77/4/1556/5864492 by guest on 31 December 2021

Acknowledgements

We thank Andrew Edwards and the anonymous reviewers for their comments.

Funding

This work was supported by the Simons Collaboration on Computational Biogeochemical Modeling of Marine Ecosystems/CBIOMES (549947 to S.S.). Additional support from the Ocean-Colour Climate-Change Initiative (OC-CCI) of the European Space Agency is gratefully acknowledged. This work is also a contribution to the National Centre for Earth Observation of the Natural Environment Research Council (UK). The work benefitted from the workshop Remote Sensing of Marine Ecosystems funded by the Croatian Ministry of Science. This work has been supported in part by Croatian Science Foundation under the project MAUD (9849).

References

Armstrong, R. A. 1994. Grazing limitation and nutrient limitation in marine ecosystems: steady state solutions of an ecosystem model with multiple food chains. Limnology and Oceanography, 39: 597–608.

Bar-On, Y. M., Phillips, R., and Milo, R. 2018. The biomass distribution on earth. Proceeding of the National Academy of Sciences of the United States of America, 115: 6506–6511.

Bouman, H. A., Platt, T., Doblin, M., Figueiras, F. G., Gudmundsson, K., Gudfinnsson, H. G., Huang, B. *et al.* 2018. Photosynthesis–irradiance parameters of marine phytoplankton: synthesis of a global data set. Earth System Science Data, 10: 251–266.

Brauer, F. 1979. Characteristic return times for harvested population models with time lag. Mathematical Biosciences, 45: 295–311.

Buitenhuis, E. T., Hashioka, T., and Quéré, L. 2013. Combined constraints on global ocean primary production using observations and models. Globlal Biogeochemical Cycles, 27: 847–858.

Cinner, J. E., and Barnes, M. L. 2019. Social dimensions of resilience in social-ecological systems. One Earth, 1: 51–56.

Edwards, C. A., Powell, T. A., and Batchelder, H. P. 1996. The stability of an NPZ model subject to realistic levels of vertical mixing. Journal of Marine Research, 11: 347–370.

Edwards, A. M., and Bees, M. A. 2001. Generic dynamics of a simple plankton population model with a non-integer exponent of closure. Chaos, Solitons and Fractals, 12: 289–300.

Edwards, A. M., Platt, T., and Sathyendranath, S. 2004. The high-nutrient, low-chlorophyll regime of the ocean: limits on biomass and nitrate before and after iron enrichment. Ecological Modelling, 171: 103–125.

Edwards, A. M., and Yool, A. 2000. The role of higher predation in plankton population models. Journal of Plankton Research, 22: 1085–1112.

Edwards, C. A., Powell, T. A., and Batchelder, H. P. 2000. The stability of an npz model subject to realistic levels of vertical mixing. Journal of Marine Research, 58: 37–370.

Eppley, R. W., Rogers, J. N., and McCarthy, J. J. 1969. Half-saturation constants for uptake of nitrate and ammonium by marine phytoplankton. Limnology and Oceanography, 14: 912–920.

Everett, J. D., Baird, M. E., Buchanan, P., Bulman, C., Davies, C., Downie, R., Griffiths, C. *et al.* 2017. Modeling what we sample and sampling what we model: challenges for zooplankton model assessment. Frontiers in Marine Science, 4: 77.

Falkowski, P. G., and Raven, J. A. 2007. Aquatic Photosynthesis, 2nd edn. Princeton University Press, Princeton.

Field, C. B. 1998. Primary production of the biosphere: integrating terrestrial and oceanic components. Science, 281: 237–240.

Friedland, K. D., Hare, J. A., Wood, G. B., Col, L. A., Buckley, L. J., Mountain, D. G., Kane, J. *et al.* 2008. Does the fall phytoplankton bloom control recruitment of Georges Bank haddock, melanogrammus aeglefinus, through parental condition. Canadian Journal of Fisheries and Aquatic Sciences, 65: 1076–1086.

Gibson, G. A., Musgrave, D. l., and Hinckley, S. 2005. Non-linear dynamics of a pelagic ecosystem model with multiple predator and prey types. Journal of Plankton Research, 27: 427–447.

Harris, G. P. 1984. Phytoplankton productivity and growth measurements: past, present and future. Journal of Plankton Research, 6: 219–237.

Hayking, S. 2005. Neural Networks: A Comprehensive Foundation, 2nd edn. Pearson Education, Singapore.

Holling, C. S. 1996. Engineering resilience versus ecological resilience. *In* Engineering within Ecological Constraints, pp. 31–43. Ed. by Schulze, P. The National Academy of Sciences, Washington.

Huisman, J., and Weissing, F. J. 1995. Competition for nutrients and light in a mixed water column: a theoretical analysis. The American Naturalist, 146: 536–564.

Huppert, A., Blasius, B., Olinky, R., and Stone, L. 2005. A model for seasonal phytoplankton blooms. Journal of Theoretical Biology, 236: 276–290.

Huppert, A., Blasius, B., and Stone, L. 2002. A model of phytoplankton blooms. The American Naturalist, 159: 156–171.

Huppert, A., Olinky, R., and Stone, L. 2004. Bottom-up excitable models of phytoplankton blooms. Bulletin of Mathematical Biology, 66: 865–878.

Izhikevich, E. M. 2007. Dynamical Systems in Neuroscience: the Geometry of Excitability and Bursting, 1st edn. MIT Press, Cambridge. doi: 10.2307/20454122.

Johnson, K. A., and Goody, R. S. 2011. The original Michaelis constant: translation of the 1913 Michaelis Menten paper. Biochemistry, 50: 8264–8269.

Kirk, J. T. O. 2011. Light and Photosynthesis in Aquatic Ecosystems, 3rd edn. Cambridge University Press, Cambridge. doi: 10.1017/CBO9780511623370.

Kovač, Z., Platt, T., Antunović, S., Sathyendranath, S., Morović, M., and Gallegos, C. 2017a. Extended formulations and analytic solutions for watercolumn production integrals. Frontiers in Marine Science, 4: 163.

Kovač, Ž., Platt, T., Ninčević Gladan, Ž., Morović, M., Sathyendranath, S., Raitsos, D., Grbec, B. *et al.* 2018a. A 55-year time series station for primary production in the Adriatic Sea: data correction, extraction of photosynthesis parameters and regime shifts. Remote Sensing, 10: 1–21.

Kovač, Ž., Platt, T., Sathyendranath, S., and Antunović, S. 2017b. Models for estimating photosynthesis parameters from in situ production profiles. Progress in Oceanography, 159: 255–266

Kovač, Ž., Platt, T., Sathyendranath, S., and Morović, M. 2016a. Analytical solution for the vertical profile of daily production in the ocean. Journal of Geophysical Research: Oceans, 121: 3532–3548.

Kovač, Z., Platt, T., Sathyendranath, S., Morović, M., and Jackson, T. 2016b. Recovery of photosynthesis parameters from *in situ* profiles of phytoplankton production. ICES Journal of Marine Science, 73: 275–285.

Kovač, Z., Platt, T., Sathyendranath, S., Morović, M., and Lomas, M. W. 2018b. Extraction of photosynthesis parameters from time series measurements of in situ production: Bermuda Atlantic time-series study. Remote Sensing, 10: 1–23.

Kulk, G., Platt, T., Dingle, J., Jackson, T., Jönsson, B. F., Bouman, H. A., Babin, M. *et al.* 2020. Primary production, an index of climate change in the ocean: satellite-based estimates over two decades. Remote Sensing, 12: 826.

Kuznetsov, Y. A. 2004. Elements of Applied Bifurcation Theory, 2nd edn. Springer, New York. doi: 10.1007/978-1-4757-3978-7.

Downloaded from https://academic.oup.com/icesjms/article/77/4/1556/5864492 by guest on 31 December 2021

Lewis, M. R., Cullen, J. J., and Piatt, T. 1984. Relationships between vertical mixing and photoadaptation of phytoplankton: similarity criteria. Marine Ecology Progress Series, 15: 141–149.

May, R. M. 1973. Stability and Complexity in Model Ecosystems, 1st edn. Princeton University Press, Princeton.

Michealis, L., and Menten, M. L. 1913. Die kinetik der invertinwirkung. Biochemistry, 49: 333–369.

Monod, J. 1949. The growth of bacterial cultures. Annual Review of Microbiology, 3: 371–394.

Pedrosa-Pamies, R., Conte, M. H., Weber, J. C., and Johnson, R. 2019. Hurricanes enhance labile carbon export to the deep ocean. Geophysical Research Letters, 46: 1–11.

Perko, L. 2001. Differential Equations and Dynamical Systems, 3rd edn. Springer, New York. doi: 10.1007/978-1-4684-0392-3.

Pimm, S. L. 1984. The complexity and stability of ecosystems. Nature, 307: 321–326.

Platt, T., and Sathyendranath, S. 2008. Ecological indicators for the pelagic zone of the ocean from remote sensing. Remote Sensing of Environment, 112: 3426–3436.

Platt, T., Broomhead, D. S., Sathyendranath, S., Edwards, A. M., and Murphy, E. J. 2003a. Phytoplankton biomass and residual nitrate in the pelagic ecosystem. Proceeding of the Royal Society A, 459: 1063–1073.

Platt, T., Gallegos, C. L., and Harrison, W. G. 1980. Photoinhibition of photosynthesis in natural assemblages of marine phytoplankton. Journal of Marine Research, 38: 687–701.

Platt, T., and Jassby, A. 1976. The relationship between photosynthesis and light for natural assemblages of coastal marine phytoplankton. Journal of Phycology, 12: 421–430.

Platt, T., Sathyendranath, S., Edwards, A. M., Broomhead, D. S., and Ulloa, O. 2003b. Nitrate supply and demand in the mixed layer of the ocean. Marine Ecology Progress Series, 254: 3–9.

Platt, T., Sathyendranath, S., and Fuentes-Yaco, C. 2007. Biological oceanography and fisheries management: perspective after 10 years. ICES Journal of Marine Science, 64: 863–869.

Platt, T., Sathyendranath, S., and Longhurst, A. 1995. Remote sensing of primary production in the ocean: promise and fulfilment. Philosophical Transactions of the Royal Society of London B, 348: 191–202.

Platt, T., Sathyendranath, S., and Ravindran, P. 1990. Primary production by phytoplankton: analytic solutions for daily rates per unit area of water surface. Proceeding of the Royal Society B, 241: 101–111.

Platt, T., White, I. I. I., White G., Zhai, L., Sathyendranath, S., and Roy, S. 2009. The phenology of phytoplankton blooms: ecosystem indicators from remote sensing. Ecological Modelling, 220: 3057–3069.

Prentice, I. C., Farquhar, G. D., Fasham, M. J. R., Goulden, M. L., Heimann, M., Jaramillo, F. J., Kheshgi, H. S. *et al.* 2001. The carbon cycle and atmospheric carbon dioxide. In Climate Change 2001: The Scientific Basis, p. 185–237. Ed. by Houghton, J. T., Ding, Y., Griggs, D. J., Noguer, M., van der Linden, P. J., Dai, X., Maskell, K., et al. Cambridge University Press, Cambridge.

Robinson, C. 1995. Dynamical Systems: Stability, Symbolic Dynamics and Chaos, 2nd edn. CRC Press.

Ryabchenko, V. A., Fasham, M. J. R., Kagan, B. A., and Popova, E. E. 1997. What causes short-term oscillations in ecosystem models of the ocean mixed layer? Journal of Marine Systems, 13: 33–50.

Sathyendranath, S., Brewin, R. J. W., Brockmann, C., Brotas, V., Calton, B., Chuprin, A., Cipollini, P. *et al.* 2019. An ocean-colour time series for use in climate studies: the experience of the ocean colour climate change initiative (OC-CCI) Sensors, 19: 4285.

Strogatz. 1994. Nonlinear Dynamics and Chaos: With Applications to Physics, Biology, Chemistry and Engineering. Perseus Books, Reading.

Sverdrup, H. U. 1953. On conditions for the vernal blooming of phytoplankton. Journal du Conseil International pour l'Exploration de la Mer, 18: 287–295.

Tilman, D., and Downing, J. A. 1994. Biodiversity and stability in grasslands. Nature, 367: 363–365.

Truscott, J., and Brindley, J. 1994. Ocean plankton populations as excitable media. Bulletin of Mathematical Biology, 56: 981–998.

Wiborg, K. F. 1976. Fishery and commercial exploitation of *Calanus finmarchicus* in Norway. Journal du Conseil International pour l'Exploration de la Mer, 36: 251–258.

Zhai, L., Platt, T., Tang, C., Sathyendranath, S., Fuentes-Yaco, C., Devred, E., and Wu, Y. 2010. Seasonal and geographic variations in phytoplankton losses from the mixed layer on the northwest Atlantic shelf. Journal of Marine Systems, 80: 36–46.

Handling editor: Matthew Oliver

Downloaded from https://academic.oup.com/icesjms/article/77/4/1556/5864492 by guest on 31 December 2021

Appendix 1

Interpretation of ξ

Consider a mixed layer extending from the surface to depth Z_m. Suppose that the nutrients are supplied to the mixed layer by a vertically advective velocity V. The supply rate will depend on the concentration difference $N_0 - N(t)$ between the mixed layer and the deep reservoir. The transport of nutrients across the base of the mixed layer is $V(N_0 - N(t))$ per unit area per unit time, with dimensions $[LT^{-1}][ML^{-3}] = [ML^{-2}T^{-1}]$. The supply has to be allocated uniformly throughout the mixed layer, such that to quantify the effect (augmentation) on the concentration there we should divide the inflow by Z_m, to yield $V(N_0 - N(t))/Z_m$ with dimensions $[ML^{-3}T^{-1}]$. It can be seen from (7) that these are the correct dimensions, from which we can identify ξ as V/Z_m, with dimensions $[T^{-1}]$. It is the ratio of the advective velocity to the depth of the mixed layer. The product $\xi(N_0 - N(t))$ is the rate of change of nutrient concentration in the mixed layer as a result of supply from below.

Now suppose that the vertical nutrient flux was diffusive rather than advective. Then we would have a diffusion coefficient with dimensions $[L^2T^{-1}]$ multiplying the concentration gradient $[ML^{-3}L^{-1}]$ giving $[ML^{-2}T^{-1}]$ as before for the flux across the base of the mixed layer, or $[ML^{-3}T^{-1}]$ after allocation over the entire mixed layer, as required by (7). In this case also, we identify ξ as a velocity (diffusive now), scaled by the mixed-layer depth, with dimensions $[T^{-1}]$. The rate of change of nutrient concentration in the mixed layer for the same vertical velocity (advective or diffusive), and the same nutrient concentration on the deep reservoir, depends on the mixed-layer depth.

Appendix 2

Stability analysis

The linearisation of the system of equations (6) and (7) reads:

$$\frac{\partial}{\partial t}\begin{bmatrix}\delta B\\ \delta N\end{bmatrix} = \mathbf{J}\begin{bmatrix}\delta B\\ \delta N\end{bmatrix}, \tag{55}$$

where the Jacobian is given as:

$$\mathbf{J} = \begin{bmatrix}\partial_B B(t) & \partial_N B(t)\\ \partial_B N(t) & \partial_N N(t)\end{bmatrix}, \tag{56}$$

with $\delta B = B(t) - B^*$ and $\delta N = N(t) - N^*$ as the perturbations of the steady state. The solution of this system is (May, 1973):

$$\begin{bmatrix}\delta B(t)\\ \delta N(t)\end{bmatrix} = c_1 \exp(\lambda_1 t)\begin{bmatrix}v_{11}\\ v_{12}\end{bmatrix} + c_2 \exp(\lambda_2 t)\begin{bmatrix}v_{21}\\ v_{22}\end{bmatrix}, \tag{57}$$

where λ_1 and λ_2 are the eigenvalues of the Jacobian, with the corresponding eigenvectors $[v_{11} \quad v_{12}]^T$ and $[v_{21} \quad v_{22}]^T$, respectively, and the constants c_1 and c_2 are set by the initial conditions:

$$c_1 = \frac{v_{22}\delta B(0) - v_{21}\delta N(0)}{v_{11}v_{22} - v_{21}v_{12}}, \tag{58}$$

$$c_2 = \frac{-v_{12}\delta B(0) + v_{11}\delta N(0)}{v_{11}v_{22} - v_{21}v_{12}}. \tag{59}$$

When both eigenvalues are negative (or have negative real parts), $\delta B(t) \to 0$ and $\delta N(t) \to 0$, meaning $B(t) \to B^*$ and $N(t) \to N^*$. In this case, the steady state is stable. When either, or both, eigenvalues are positive, or have a positive real part, the system is unstable. In addition, when the imaginary part of the eigenvalues is distinct from zero, $B(t)$ and $N(t)$ oscillate and the imaginary part of the eigenvalues determines the frequency of these oscillations.

To get the eigenvalues of the Jacobian, we need to find the roots of its characteristic polynomial:

$$x^2 - \mathrm{Tr}\mathbf{J}\, x + \det\mathbf{J} = 0, \tag{60}$$

which are given as:

$$\lambda_{1,2} = \frac{1}{2}\mathrm{Tr}\mathbf{J} \pm \frac{1}{2}\sqrt{(\mathrm{Tr}\mathbf{J})^2 - 4\det\mathbf{J}}. \tag{61}$$

As was demonstrated in Stability of the steady state section for the system of (6) and (7), the determinant of the Jacobian is positive ($\det\mathbf{J} > 0$) and the trace is negative ($\mathrm{Tr}\mathbf{J} < 0$). This reflects on the eigenvalues and stability in the following way. When we have $(\mathrm{Tr}\mathbf{J})^2 < 4\det\mathbf{J}$, the eigenvalues are complex conjugate and the sign of the trace determines stability. Since it is negative the system is stable. The other case is of $(\mathrm{Tr}\mathbf{J})^2 > 4\det\mathbf{J}$. Given that now $\sqrt{(\mathrm{Tr}\mathbf{J})^2 - 4\det\mathbf{J}} < |\mathrm{Tr}\mathbf{J}|$ and $\mathrm{Tr}\mathbf{J} < 0$, both eigenvalues are negative and therefore the system is stable in this case also. In both these cases, if the trace was positive the system would be rendered unstable. Therefore, it has to be negative for the system to be stable. Also, if the determinant was negative we would have $\sqrt{(\mathrm{Tr}\mathbf{J})^2 - 4\det\mathbf{J}} > |\mathrm{Tr}\mathbf{J}|$, giving $\lambda_1 > 0$ and $\lambda_2 < 0$. This steady state is classified as a saddle point and is unstable since one eigenvalue is positive. Therefore, the determinant needs to be positive for the system to be stable.

Appendix 3

General characteristic return times

The characteristic return time is given simply by the real part of the eigenvalues of the Jacobian. When the imaginary part of the eigenvalues is non-zero, meaning the steady state is a spiral sink and oscillations emerge, the real part of both eigenvalues is equal to:

$$\mathrm{Re}(\lambda_{1,2}) = \frac{1}{2}\left(B^*\partial_B\langle P^B\rangle_{Z_m,T} - \nu\partial_N\langle P\rangle_{Z_m,T} - \xi\right), \tag{62}$$

and the characteristic return time is therefore:

$$T = 2/|B^*\partial_B\langle P^B\rangle_{Z_m,T} - \nu\partial_N\langle P\rangle_{Z_m,T} - \xi|. \tag{63}$$

There is only one characteristic return time because the real parts of both eigenvalues are the same. The eigenvalues come as a complex conjugate pair and their imaginary part determines the oscillation frequency. The period of the oscillations is given as:

$$T = \frac{4\pi}{|\sqrt{(\mathrm{Tr}\mathbf{J})^2 - 4\det\mathbf{J}|}}, \tag{64}$$

where the trace $\mathrm{Tr}\mathbf{J}$ is given by (21) and the determinant $\det\mathbf{J}$ by (24). The same does not apply for the case of a sink node steady

Downloaded from https://academic.oup.com/icesjms/article/77/4/1556/5864492 by guest on 31 December 2021

state. In this case, both eigenvalues are real and $(\mathrm{Tr}\mathbf{J})^2 - 4\mathrm{det}\mathbf{J} > 0$ is satisfied. Now we find two characteristic return times:

$$T_1 = 2/(\mathrm{Tr}\mathbf{J} + \sqrt{(\mathrm{Tr}\mathbf{J})^2 - 4\mathrm{det}\mathbf{J}}), \tag{65}$$

and

$$T_2 = 2/(\mathrm{Tr}\mathbf{J} - \sqrt{(\mathrm{Tr}\mathbf{J})^2 - 4\mathrm{det}\mathbf{J}}), \tag{66}$$

where the trace $\mathrm{Tr}\mathbf{J}$ is given by (21) and the determinant $\mathrm{det}\mathbf{J}$ by (24). Shading and nutrient limitation now acting together results in a somewhat complicated expression for the characteristic return times when fully expanded.

Appendix 4

Average mixed-layer production

It is simple to show that $\langle P\rangle_{Z_\mathrm{m},T} = \langle P_T(z)\rangle$, where $P_T(z)$ is the daily production profile (Kovač *et al.*, 2016a, 2017b) and $\langle P_T(z)\rangle$ marks the vertical average of the daily production profile in the mixed layer. Acknowledging this, we have the following expression for the derivative of average mixed-layer production with respect to Z_m:

$$\partial_{Z_\mathrm{m}}\langle P\rangle_{Z_\mathrm{m},T} = \frac{1}{24\chi}\partial_{Z_\mathrm{m}}\left(\frac{1}{Z_\mathrm{m}}\int_0^{Z_\mathrm{m}} P_T(z)\mathrm{d}z\right). \tag{67}$$

Upon taking the derivative we obtain:

$$\partial_{Z_\mathrm{m}}\langle P\rangle_{Z_\mathrm{m},T} = \frac{1}{24\chi Z_\mathrm{m}}\left(\partial_{Z_\mathrm{m}}\int_0^{Z_\mathrm{m}} P_T(z)\mathrm{d}z - \frac{1}{Z_\mathrm{m}}\int_0^{Z_\mathrm{m}} P_T(z)\mathrm{d}z\right), \tag{68}$$

which, acknowledging:

$$\partial_{Z_\mathrm{m}}\int_0^{Z_\mathrm{m}} P_T(z)\mathrm{d}z = P_T(Z_\mathrm{m}), \tag{69}$$

and:

$$\int_0^{Z_\mathrm{m}} P_T(z)\mathrm{d}z = \langle P_T(z)\rangle Z_\mathrm{m}, \tag{70}$$

reduces to:

$$\partial_{Z_\mathrm{m}}\langle P\rangle_{Z_\mathrm{m},T} = \frac{1}{24\chi Z_\mathrm{m}}(P_T(Z_\mathrm{m}) - \langle P_T(z)\rangle). \tag{71}$$

Because the production profile is a decreasing function of depth for a uniform biomass profile (Kovač *et al.*, 2016a), the production at the base of the mixed layer $P_T(Z_\mathrm{m})$ will be less than the average production in the mixed layer $\langle P_T(z)\rangle$, therefore $P_T(Z_\mathrm{m}) - \langle P_T(z)\rangle < 0$, meaning that mixed-layer deepening will be followed by a decrease in average mixed-layer production, and mixed-layer shallowing by an increase in average mixed-layer production.

Appendix 5

Generic model

The model presented is written in a historical notation, which already has a long and continuous application and which is parameter specific. However, to achieve generality we provide also a more generic version of the model with simplified notation:

$$\frac{\mathrm{d}B}{\mathrm{d}t} = P\frac{N}{N+N_k}B - LB, \tag{72}$$

$$\frac{\mathrm{d}N}{\mathrm{d}t} = -\nu P\frac{N}{N+N_k}B + \xi(N_0 - N), \tag{73}$$

where $P = P(I_0^m, Z_\mathrm{m}, B, K_w, k_B)$. Multiple functional forms can be taken for P. The one used in this paper stems from the work of Platt *et al.* (1990) and is given in (4) and in many subsequent papers.

Downloaded from https://academic.oup.com/icesjms/article/77/4/1556/5864492 by guest on 31 December 2021